ICAS 2016
30th Congress of the International Council of the Aeronautical Sciences
DCC, Daejeon, Korea : September 25-30, 2016

NUMERICAL AND EXPERIMENTAL RESEARCH ON AERODYNAMICS OF A HIGH-SPEED PASSENGER VEHICLE WITHIN THE HEXAFLY-INT PROJECT

J. Steelant[*], V. Villace[*], M. Marini[**], G. Pezzella[**], B. Reimann[†], S.L. Chernyshev[‡], A.A. Gubanov[‡], V.A. Talyzin[‡], N.V. Voevodenko[‡], N.V. Kukshinov[§], A.N. Prokhorov[§], A.J. Neely[¶], C. Kennell[¶], D. Verstraete[‖], D. Buttsworth[ǂ]
[*]ESA-ESTEC, [**]CIRA, [†]DLR, [‡]TsAGI, [§]CIAM, [¶]Univ. of New South Wales, [‖]Univ. of Sydney, [ǂ]Univ. of Southern Queensland

Keywords: *hypersonic vehicle, aerodynamics, glider, scramjet propulsion, experiments*

Abstract

Hypersonic passenger transport is intrinsically linked to long-haul intercontinental flights. Its development and deployment will demand an international approach. The internationally funded HEXAFLY-INT project is a first step into this direction. Key elements for civil high-speed transportation are jointly developed towards an experimental flight. The present paper describes the various numerical and experimental investigations carried out so far by the different international partners.

1 Introduction

The overall aim of the European Community (EC) co-funded HEXAFLY-INT international project with partners from Europe, Russian Federation and Australia is to design, manufacture and flight test a high-speed vehicle, based on the configuration developed in previous EC co-funded projects ATLLAS I & II [1][2], LAPCAT I & II [3][4], and HEXAFLY [5][6]. Under HEXAFLY-INT, both a glider and a propelled variant of the high-speed vehicle are being considered, the former being developed by EC partners with international partners, the latter being developed only by the Russian partners. The flight experiment carried out by the Europeans, Russians and Australians, is focused on a self-controlled glider with several breakthrough technologies on-board [7], demonstrating its aerodynamic efficiency and collecting valuable aerodynamic, control and aero-thermo-structural flight data to validate the methods and technologies used to design the hypersonic vehicle [7][8][9][10].

The Experimental Flight Test Vehicle (EFTV) will be launched by a sounding rocket (the Brazilian VS43 launcher equipped by an 8-ton solid rocket motor) in a suborbital trajectory having an apogee at about 90 km. After the release from the launcher, the EFTV will perform the first part of the descent docked to the Experimental Service Module (ESM), which controls the vehicle attitude. As soon as the EFTV features full aerodynamic control authority, it undocks from the ESM and pulls up from its descent to perform a hypersonic cruise at approximately Mach 7. In this experimental phase, the EFTV aims to demonstrate a high aerodynamic efficiency ($L/D \geq 4$), a positive aerodynamic balance at controlled cruise Mach numbers ($7 \div 8$), an optimal use of advanced high-temperature materials and structures, and potentially the evaluation of the sonic boom impact by deploying dedicated ground measurement equipment.

Both the glider and the propelled options of the HEXAFLY-INT high-speed vehicle are characterized from the aerodynamic and aerothermodynamic points of view. Numerical and experimental research progress is described in the following.

2 The Glider Vehicle Aerodynamics

2.1 The Experimental Flight Test Vehicle

The EFTV, see Fig. 1, is a hypersonic glider 3.29m long and with a span of about 1.23m. The EFTV has a two-dimensional nosetip with 2mm rounding and 2mm lateral fillet, while the wing is characterized by a 80° sweep angle and 14°

negative dihedral angle, and 1mm rounded leading edge. As control surfaces, the vehicle is equipped by a couple of active ailerons (0.4m long and 0.32m wide), which can be deflected in symmetric and asymmetric way, and a couple of fixed vertical fins characterized by a 68.5° sweep angle and a 54° angle formed between the two fins in the transversal plane. The present aeroshape is the result of an evolution [8] that, following the suggestions by the continuous aero-heating assessment, has impacted mainly the nosecap and forebody configuration, the wing (leading edge and fuselage intersection) and the aileron.

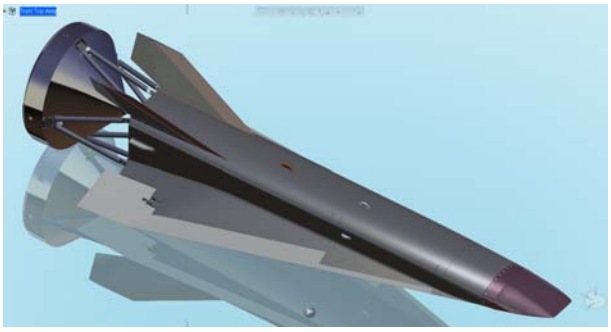

Fig. 1. The EFTV glider with ESM.

As general material layout, the cold structure of the EFTV is in titanium alloy, as well as all the fuselage and wing panels with the exception of the copper nose section. Wing leading edges and ailerons are in C/C-SiC, while the vertical tails in titanium are built with copper for the leading edges. The metallic exposed surface parts are thermally protected by a ZrO_2 coating with a proper optimized thickness. This material layout is compliant with the aerothermal loading conditions expected for the glider.

The EFTV will be equipped with an avionic system composed by an inertial measurement unit, a GPS, two servo-actuators for the ailerons, and a flight control computer, which will ensure the on-board mission management. The vehicle will also be equipped with an in–flight measurement system acquiring pressure, temperature and acceleration data sensors for the sake of post flight analysis and simulation tools validation. The on-board avionics will also include a downlink telemetry system (i.e. with antennas) which will transmit all mission data to the Ground Control Station at the launch site.

2.2 Vehicle Aerodynamic Appraisal

EFTV's aerodynamics is being developed by means of both numerical and experimental approaches, as discussed hereinafter.

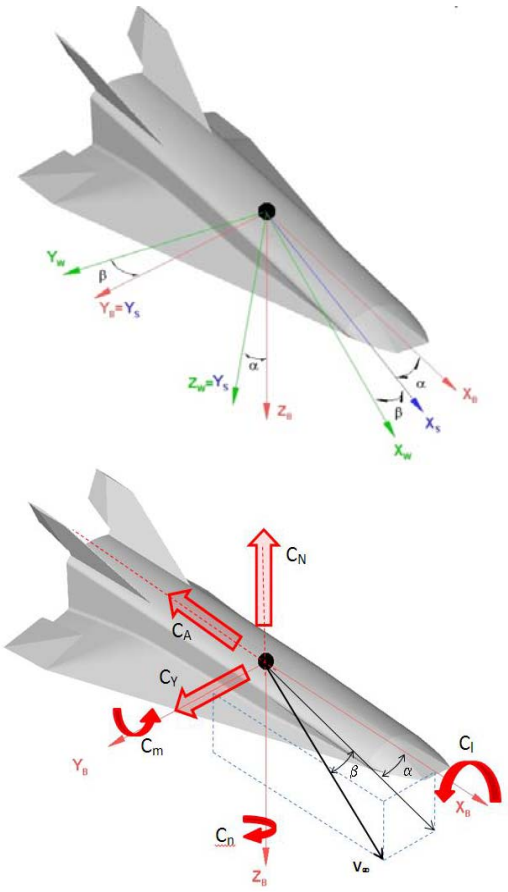

Fig. 2. Glider WRF and BRF (top); and BRF with aerodynamic coefficients convention (down).

This appraisal is addressed in terms of lift (C_L), drag (C_D), side force (C_Y), rolling moment (C_l), pitching moment (C_m) and yawing moment (C_n) coefficients, defined according to ISO 1151, see Fig. 2. The moment reference center (MRC) coordinates in the Layout Reference Frame (LRF) for the EFTV are (1.455, 0.0, 0.12) [m]. In particular, C_L and C_D are provided in the vehicle's Wind Reference Frame (WRF, X_w, Y_w, Z_w), while C_Y, C_l, C_m, and C_n are evaluated in the vehicle's Body Reference Frame (BRF, X_B, Y_B, Z_B), see Fig. 2.

The reference geometric parameters are: L_{ref}=3.29m (i.e. body length/longitudinal reference length); b_{ref}=1.24m (i.e. wing span/lateral-directional reference length); S_{ref}=2.52m^2 (i.e. vehicle planform area/reference area).

2.3 CFD Activities and Results

Vehicle numerical aerodynamics relies on several CFD analyses carried out by DLR, CIRA, ESA and TsAGI. In the early design phase only inviscid CFD computations were performed and a preliminary AErodynamic DataBase (AEDB) of EFTV configuration (i.e. FC4 aeroshape) was setup by DLR-Braunschweig [8] with the goal to provide aerodynamic performance for the first Flight Mechanics analyses. In fact, it had to be verified that vehicle aerodynamic surfaces were able to provide lift at hypersonic atmospheric entry to stay within the load constraints during descent. Aerodynamic coefficients were provided as a function of Mach number, angle of attack, sideslip angle, and aileron deflections. In particular, the AEDB was setup by performing a massive number of computations (more than 1700 inviscid CFD simulations) by using the DLR code TAU [11]. This allowed focusing on some critical design aspects not predictable with simplified tools without increasing too much the computational effort, like vehicle longitudinal and lateral-directional static stability.

The Mach range from 2 to 9 was analyzed for the EFTV only in continuum regime with air modelled as an ideal gas. This latter assumption was still valid considering that the highest Mach number is equal to 9 and, in particular, because of the very slender EFTV configuration (leading edge radius O(mm) for nosetip, wings and fins) that shall fly at rather low angles of attack and with weak attached shock waves.

An example of inviscid aerodynamic assessment is shown in Fig. 3. As summarized in Ref. [8], the EFTV aeroshape features rather high lift-to-drag ratios (L/D) at hypersonic speeds, and no significant effects of sideslip on aerodynamic efficiency and total pitching moment for both clean and deflected aileron configuration were predicted. Numerical results clearly underline that the glider is statically stable in longitudinal flight at all Mach numbers under investigation and for all the angles of attack, sideslip, and aileron deflections considered so far.

Further, results also point out that the aeroshape seemed to be trimmable in all the flight conditions investigated [8], also for supersonic Mach numbers and higher angles of attack. Finally, static stability in lateral-directional flight conditions is also confirmed since, with the provided MRC, at all Mach numbers it is verified that $C_{Y\beta}<0$, $C_{n\beta}>0$ and $C_{l\beta}<0$ (the last one only for positive angles of attack) [8].

As a conclusive result, the preliminary AEDB pointed out the compliance of hypersonic glider's aerodynamic performance with the expected flight envelope [8].

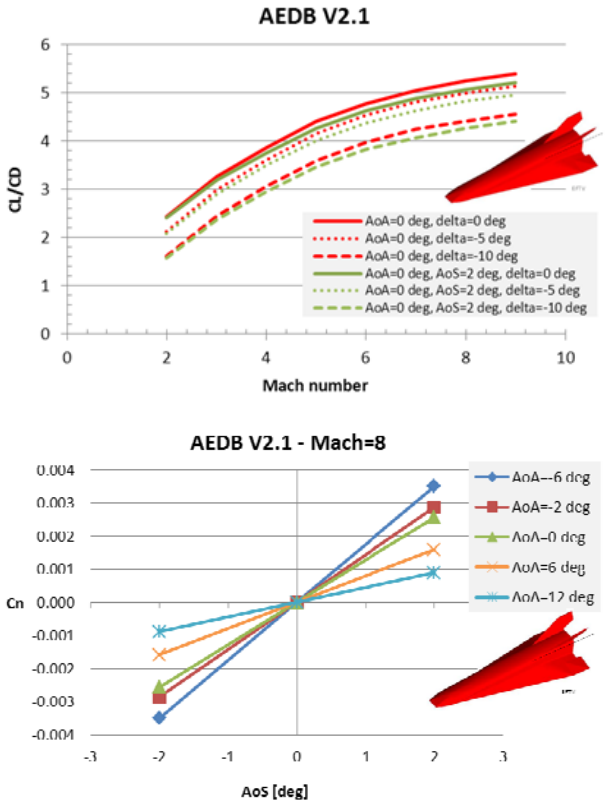

Fig. 3. The L/D versus Mach (top) and yaw moment coefficient versus sideslip (bottom) at different attitudes.

The preliminary mission trajectory was generated by DLR-Moraba for what concerns the VS43 launch vehicle, assuming a total payload mass of 800kg (EFTV, ESM, launch vehicle service module, fairing), and by Gas Dynamics Ltd. (GDL) for both the descending "train" EFTV+ESM and the EFTV alone after the separation from ESM, assumed at 50km of altitude, up to 20km of altitude. The hypothesis of continuum regime was also verified for the last two phases of flight trajectory.

A number of 3 degree-of-freedom (DoF) planar trajectories were generated for the

hypersonic glider, based on the inviscid AEDB. A viscous correction was added only to the axial force coefficient C_A (during the trimmed aerodynamics/trajectory calculation) by means of an engineering estimation of viscous forces acting on the vehicle, considered as a flat plate with a total wetted area of 7.35m^2. The skin-friction coefficient was evaluated for a compressible turbulent boundary layer using the reference temperature method (Schoenherr correlation), i.e.

$$C_f = 0.455 \frac{\rho_r}{\rho_e} \log_{10}\left(\frac{\rho_r u_e L}{\mu_r}\right)^{-2.58} \quad (1)$$

In Eq. (1) r stands for conditions evaluated at the turbulent reference temperature, e for free-stream conditions.

For the trajectory calculation, an EFTV mass of 350 kg was assumed with a center of gravity coinciding with the MRC, i.e. at 57% of the glider full length. EFTV's AoA initial schedule was based on a profile defined by CIRA that satisfies control authority criteria.

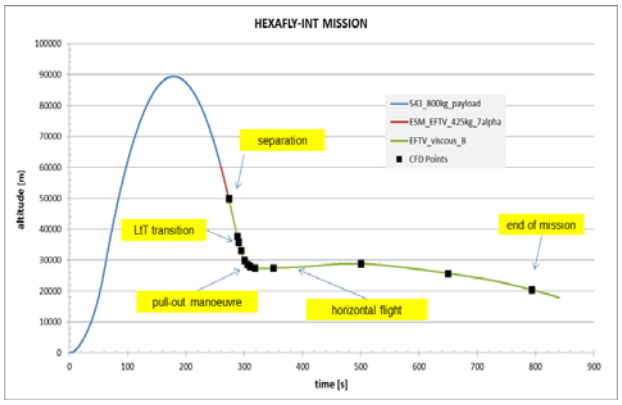

Fig. 4. Reference trajectory: altitude time history.

Trajectory labelled B-viscous (see Fig. 4) was finally selected as reference, being the lower reference trajectory of the flight corridor having a built-in margin during future trajectory consolidation, and preliminary EFTV/ESM separation has been fixed at 50km altitude to satisfy typical control authority criteria.

CIRA, ESA and TsAGI are currently carrying out Navier-Stokes (NS) CFD simulations to generate the final viscous AEDB, which will include also the model of uncertainties for aerodynamics and the dynamic derivatives data-package, thus providing inputs for flight mechanics, thermo-structural analysis (the aero-thermal loading conditions the EFTV has to withstand during the flight must be accurately verified) and in-flight experimentation layout optimization.

The complete CFD test matrix foresees 236 3-D Navier-Stokes simulations in laminar and fully turbulent flow conditions with air as ideal gas. A temperature-dependent formulation is being considered for the specific heat at constant pressure (i.e. thermally perfect gas) to accommodate the rather high flow energy, Sutherland's relationship is being used for the dynamic viscosity, and Spalart-Allmaras one-equation eddy viscosity is being selected for turbulence modelling. ESA is using DLR's TAU code [11], while CIRA and TsAGI are using ANSYS-FLUENT commercial code.

Those CFD simulations are conceived to address the effects of Mach number, angle of attack, angle of sideslip, symmetric and asymmetric aileron deflection, Reynolds number, grid resolution, turbulence models, laminar-to-turbulent transition, code-to-code, and finally to verify trim conditions and aero-thermal loads along the reference trajectory.

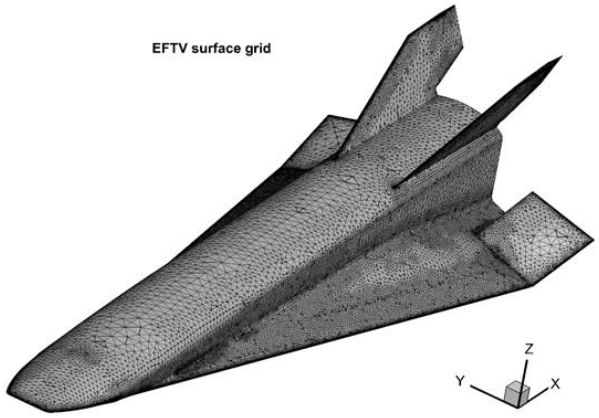

Fig. 5. Hybrid NS mesh.

An exemplary hybrid computational grid (i.e. tetrahedrons in the flow and prisms inside the boundary layer) built for NS simulations is shown in Fig. 5. At least 10 millions of cells were necessary for a half configuration, and in case of turbulent boundary layer assumption the condition of Y+=O(1) at wall was imposed.

Surface temperature contours on the full vehicle at 29.93km altitude during the descent

are shown in Fig. 6. The hot nosetip, wing leading edges and fin leading edges as result of nearly attached shock waves are noticeable. Further, the colder upper panels of fuselage and wings and fin portside due to high angle of attack (12°) of this particular flight condition as well as the hotter leeside of the aileron that is deflected negatively to trim the EFTV (-15.72°) are also evident. The effect of sideslip at high angle of attack, at Mach=7.5 and in clean configuration, is also shown in Fig. 7.

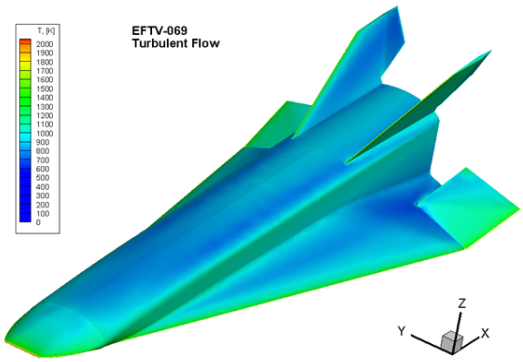

Fig. 6. EFTV surface temperature contours (29.93km, Mach=7.25, AoA=12°, Aileron=-15.72°).

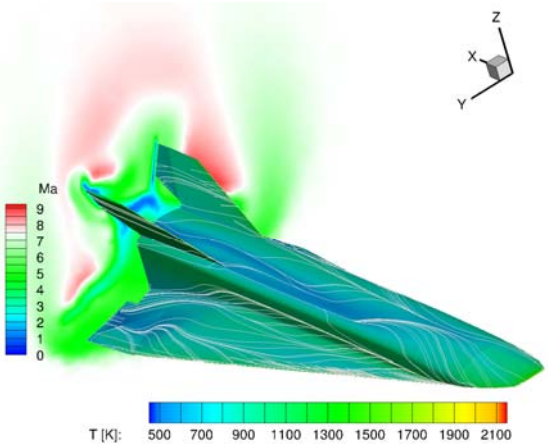

Fig. 7. EFTV surface temperature contours and skin-friction lines (Mach=7.5, AoA=10°, AoS=4°, clean configuration).

From laminar boundary layer parameters extracted from CFD results to apply local natural and step-induced transition criteria along the reference trajectory, a fully turbulent flow was expected at the altitude of about 30 km.

Computed results in terms of aerodynamic force and moment coefficients, along the reference trajectory, are shown in Fig. 8 and Fig. 9, where also the "trimmed" aerodynamic coefficients (C_m=0) extracted by trajectory B-viscous are reported for comparison purposes.

This has been done in order to cross-check the reliability of the method used by GDL for the trajectory generation.

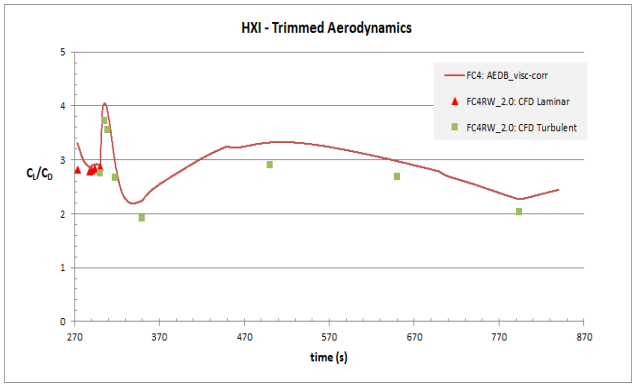

Fig. 8. EFTV trimmed aerodynamics: aerodynamic efficiency.

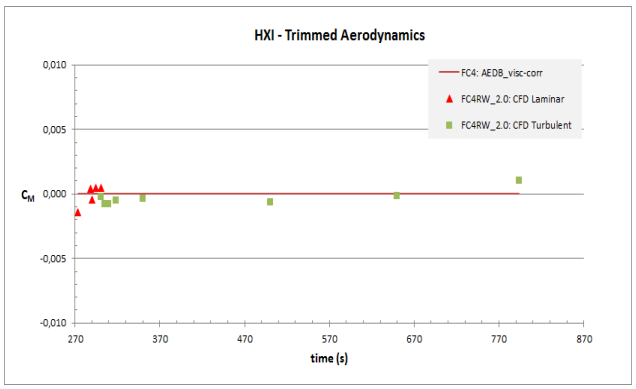

Fig. 9. EFTV trimmed aerodynamics: pitching moment coefficient.

A general good agreement between CFD results and AEDB results with viscous correction along the reference trajectory is observed, even though this latter approach, as expected, overestimates lift coefficient C_L (max. +10.9%) and aerodynamic efficiency C_L/C_D (max. +14.6%), whereas drag coefficient C_D is underestimated (max. -13,7%). From Fig. 9, it is evident that trimmed conditions along the reference trajectory are nearly similar for all the investigated flight conditions.

2.4 TsAGI Aerodynamic Tests on the EFTV Glider Option

The experimental test campaign on the aerodynamics of the EFTV glider configuration were performed at TsAGI in the supersonic and hypersonic wind tunnel T-116, characterized by

a test chamber with a squared cross section of 1 m × 1 m size. The tests were performed with the model produced by TsAGI, whose scale was 0.35 w.r.t. the size of the EFTV. The model (Fig. 10) has allowed investigating aerodynamic characteristics of the vehicle with different settings of aileron's deflection.

Fig. 10. The model of the EFTV Glider Option.

M	3.03	4.05	5.05	6.00	6.99	7.88
P_{tot}, atm	1.1	1.4	5	7.4	22	31.5
T_{tot}, K	300	300	455	485	675	825
Re_{1M} *10^{-6}	7.74	5.96	6.88	6.32	7.66	5.92
Simulated Flight Altitudes:						
H, km	24.8	28	28.4	30.5	30	32.5

Tab. 1. Flow conditions used in the Wind Tunnel T-116.

The tests have been performed in the Mach number range from 3 to 8 at angles-of-attack (AoA) from – 6º to 12º. The flow parameters realized at these tests are reported in Tab. 1. First test results for aerodynamic efficiency L/D (Mach=3÷8, clean configuration) and pitching moment coefficient C_m (Mach=7, ailerons symmetrically deflected) are shown in Fig. 11 and Fig. 12, respectively.

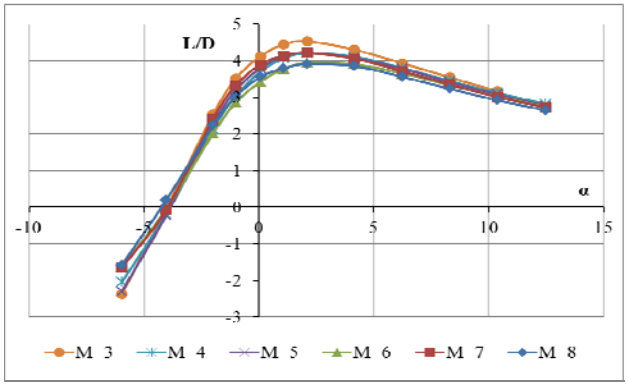

Fig. 11. Aerodynamic Efficiency L/D of the glider model.

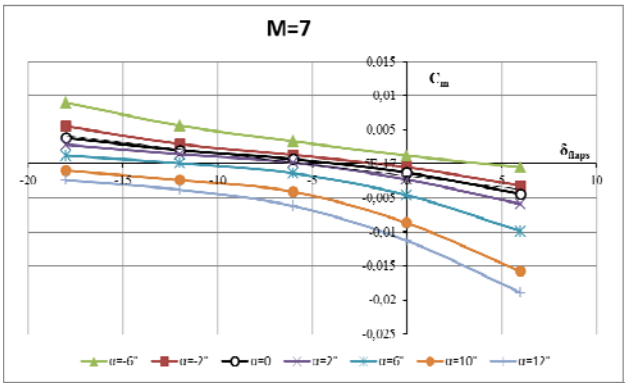

Fig. 12. Pitching Moment Coefficient C_m of the glider model.

Preliminary comparisons among numerical (inviscid AEDB with viscous correction) and experimental results for vehicle aerodynamics are provided hereinafter. For instance, data comparisons for axial force coefficient at Mach=4 and 7 are shown in Fig. 13. The AEDB viscously corrected (see Eq. (1)) with the wind tunnel conditions, agrees quite well with the experimental and numerical data.

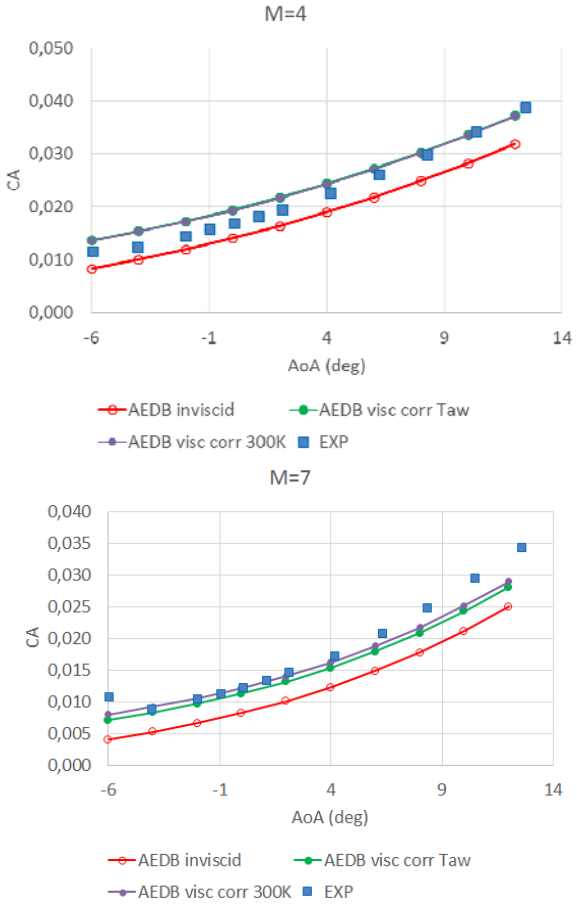

Fig. 13. Axial force coefficient at M=4 and 7. Comparison among numerical and experimental data.

At the time of writing, TsAGI is going to start some experimental tests devoted to hypersonic boundary layer transition, with two different transition grit concepts installed at the nose/fuselage junction, to complete the experimental campaign.

2.5 EFTV/ESM Separation Aerodynamics

Simulations of the separation between EFTV and ESM have been performed by DLR-Braunschweig by using a strong coupling cycle between rigid body motion and aerodynamic loads, implemented in the in-house CFD code TAU [11]. For moving grids TAU is written in an arbitrary Eulerian-Lagrangian formulation. The technique of overlapping grids is an important feature to simulate configurations with movable parts. The method handles the data exchange in the overlapping region. For the presented simulations with moving bodies, the motion is separately solved in the Rigid Body Dynamics (RBD) module solving Newton's second law and the Euler equation of rotational dynamics. The coupled CFD/RBD problem is solved in a partitioned manner. A so-called strong coupling scheme is used: the coupled equations are iteratively solved within every physical time step by repeatedly solving the involved disciplines CFD and RBD separately based on the exchanged coupling quantities. These are on CFD side aerodynamic loads (forces, moments) and on RBD side the motion state (position, velocities). Fig. 14 shows the operation chart of a strongly coupled simulation.

The separation of the ESM was simulated for altitudes of 60 km and 40 km at a Mach number of 8, angle of attack of 7° and an angle of sideslip of 0° and 2°. The flight path angle is taken from reference trajectory, whilst the struts connecting ESM to EFTV are neglected. Fig. 15 shows the computational domain for the separation simulations. Fig. 16 shows two snap-shots from the unsteady coupled simulation. The surface color is an indicator for the wall pressure. Shock waves are visualized by using a numerical pseudo-Schlieren method. Fig. 17 shows the horizontal and vertical position of the CoG of the ESM versus time. At 40 km the effect of the aerodynamic forces is dominant, while at 60 km the motion is dominated by gravity. Further studies of the separation process at 55 km altitude, including the connection between EFTV and ESM, are planned.

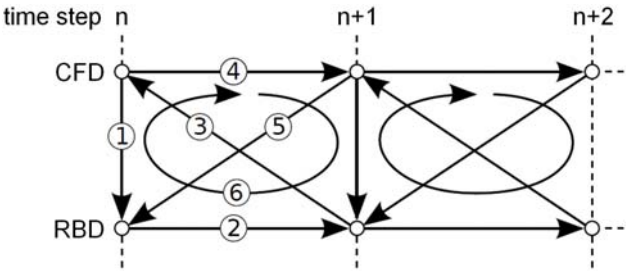

Fig. 14. CFD/RBD coupling scheme.

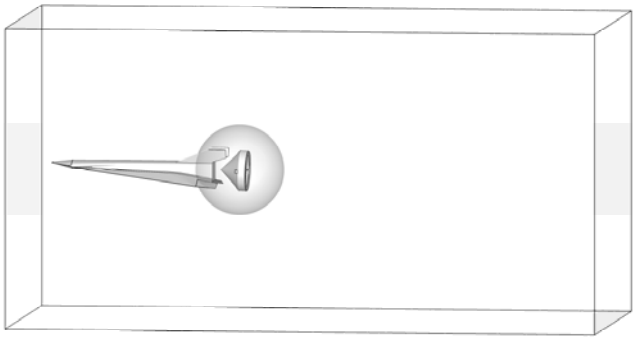

Fig. 15. Computational domain for separation simulations.

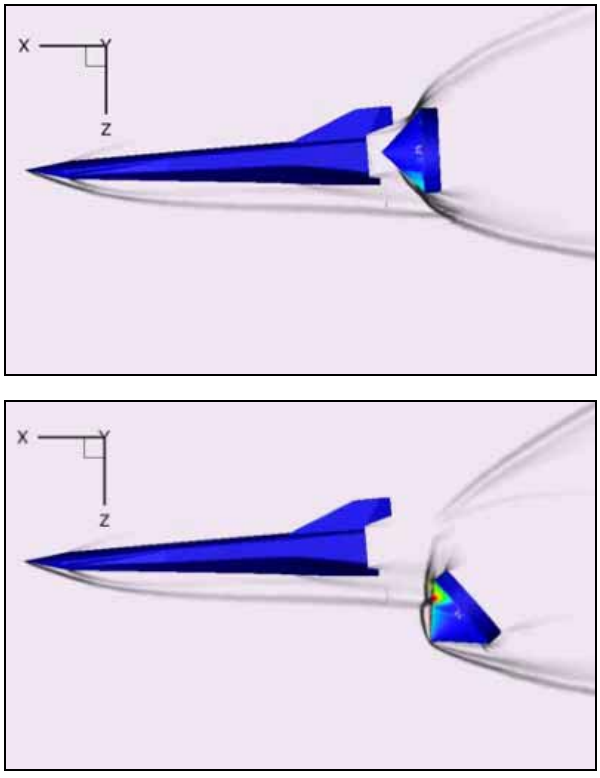

Fig. 16. Flow field during separation at 60 km altitude.

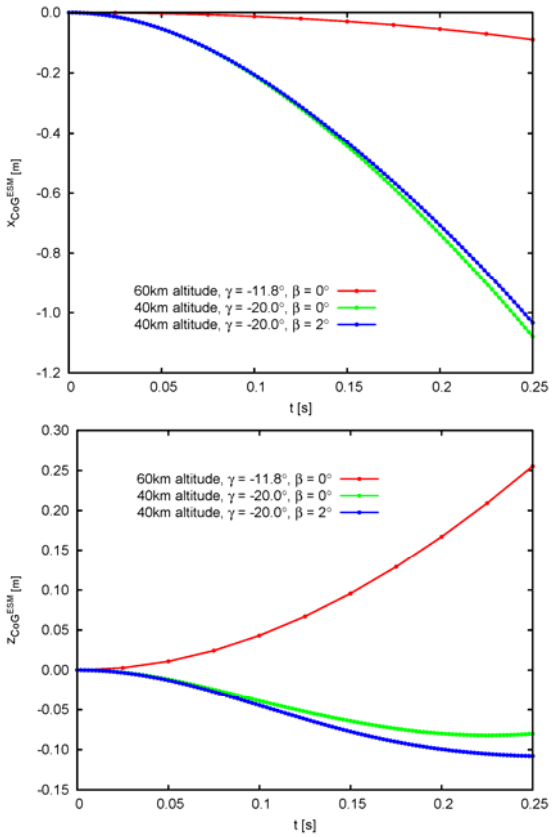

Fig. 17. Horizontal and vertical position of the CoG of the ESM during separation for different trajectory points.

Separation dynamics analysis were carried out preliminarily also by CIRA [12].

2.6 Subsonic Handling Qualities

As the project foreshadows a high-speed passenger vehicle [13], the EFTV needs to be stable throughout the entire flight envelope. Even though subsonic stability is often overlooked in hypersonic vehicles, it is crucial to obtain a viable final design. The low speed stability of the vehicle is currently investigated by University of Sydney through a combination of wind tunnel testing and CFD.

Fig. 18 shows results of the CFD simulations by ANSYS-FLUENT at 30 m/s (wind tunnel test conditions) at various angles of attack. The formation of vortices is clearly predicted, which results in a highly non-linear lift curve, and those vortices might cause an unstable pitch break around AoA=10 deg which could affect the landing speed of the vehicle.

As the lateral stability of highly swept wings is dominated by uneven vortex breaking on the wind- and leeward side, simulations were also run at different sideslip angles. Fig. 19 indicates that lateral handling is dominated by uneven vortex strengths under sideslip effects. Whereas the difference in vortex strength increases at higher AoA, the vehicle is found to be stable at sideslip angles up to 10 degrees.

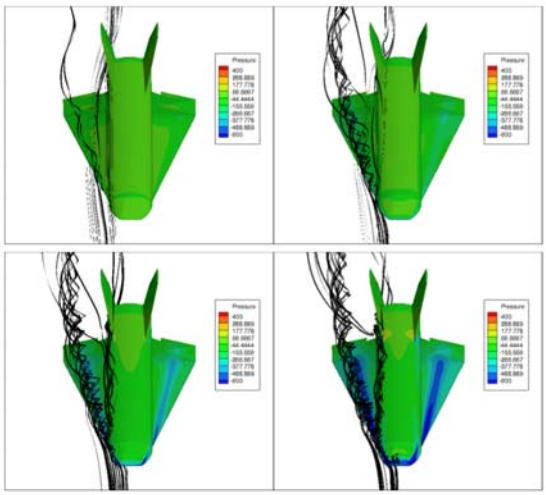

Fig. 18. Contours of pressures [Pa] and streamlines showing vortex formations at AoA=0, 5, 10 and 15 deg.

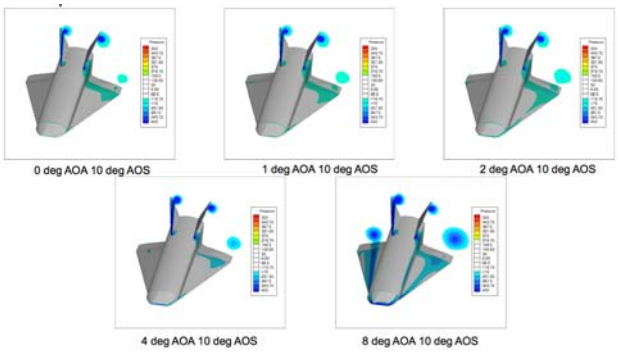

Fig. 19. Uneven vortex strength under sideslip conditions.

Finally, it was found that at high sideslip conditions the vortex of the nose cone could either stay attached at the wind leading edge or detach. Fig. 20 shows CFD and smoke tunnel visualization of the nose vortex and flow spillage over the body, confirming that the CFD simulations capture the dominant flow features.

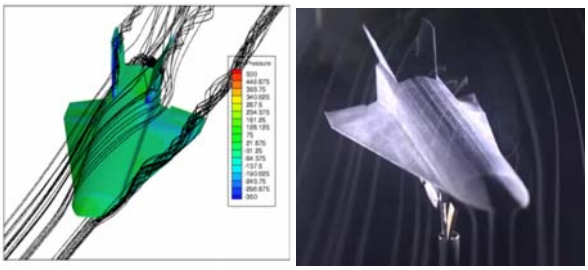

Fig. 20. Nose vortex at high sideslip angles.

3 Experimental Validation of Aerodynamic Database

University of New South Wales (UNSW) and University of Southern Queensland (USQ) have been developing a method to measure the aerodynamics of high-speed vehicles by free flying them in ground test facilities [14]. This provides a relatively cost-effective and time-efficient approach to the validation of the numerically derived aerodynamic database of a high-speed flight-test design.

3.1 Free flight technique

A dynamically scaled model of EFTV is manufactured at sub-scale, instrumented with a miniaturized onboard inertial measurement unit (IMU), and flown in the short duration flow of a hypersonic wind tunnel while being filmed by a high-speed schlieren optical visualization tool.

Different 1/13 scale models of the EFTV have been manufactured either using 3D-printed PLA (polylactide) or in a hybrid construction using an NC-machined aluminium fuselage with 3D-printed PLA wings and fins. The latter allows the straightforward changeover of wings incorporating different flap deflection angles.

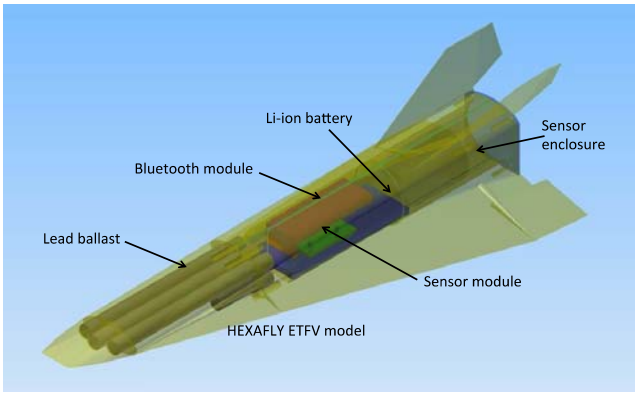

Fig. 21. Schematic layout of the EFTV model instrumented with internal IMU.

The miniaturized IMU incorporates a tri-axial accelerometer and a tri-axial gyroscope as well as a dedicated microcontroller, power supply and blue-tooth module for communication. Internal ballast is used to tune the mass, CoG and moments of inertia of the model to ensure that the EFTV model is dynamically scaled [15] (see Fig. 21).

A number of experimental campaigns were performed in the University of Southern Queensland's hypersonic wind tunnel (TUSQ) [16]. This compression-heated Ludwieg tunnel provides approximately 200ms of steady flow, with a start-up period of around 5ms. The Mach 6 nozzle produces an inviscid core flow of 160mm. The model is released to fall under gravity toward the centerline of the Mach 6 nozzle, and then the tunnel is fired to produce the test flow in which the model then flies. The Schlieren system provides both high-speed video for image tracking and simultaneous visualization of the flow structure around the model during the flight (see Fig. 22).

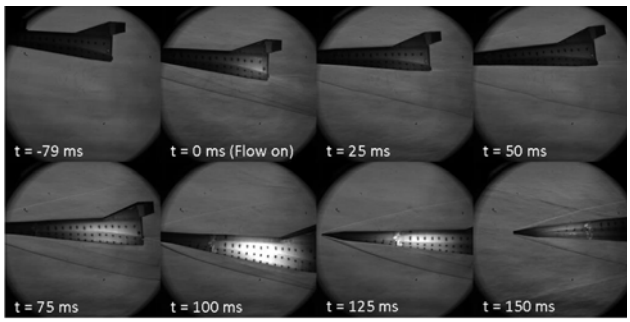

Fig. 22. Selected frames from the high-speed video showing Schlieren visualization of the flow structure around the free-flying model [14].

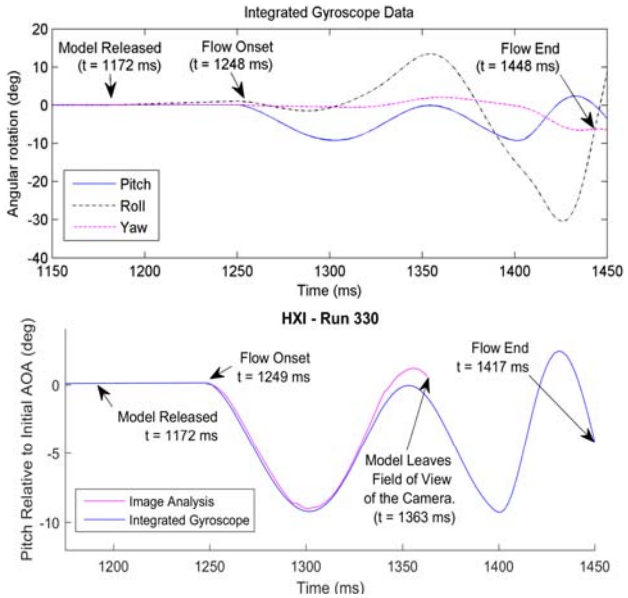

Fig. 23. (a) Pitch, roll and yaw rotations relative to the model's initial position. (b) Comparison of pitch rotation from image processing and gyroscope data [14].

Fig. 23 shows example data from a single flight of the EFTV model including comparison between the IMU and image tracking data.

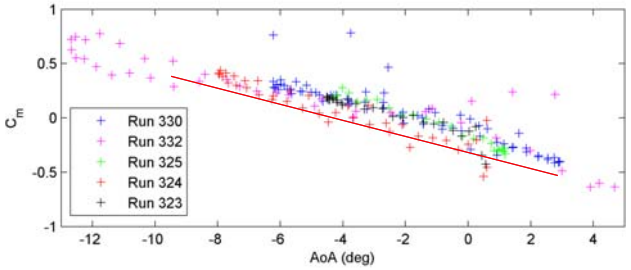

Fig. 24. Comparison between TAU inviscid computation (red line, by DLR) and free flight data from TUSQ runs.

Initial comparison of the experimental data from the scaled free flight tests and equivalent dynamic numerical simulations indicate good agreement, see Fig. 24.

3.2 EFTV/ESM Separation studies

The free flight technique is also being adapted to investigate the aerodynamics of the separation of the EFTV and the ESM during the descent through the atmosphere. Initial proof-of-concept experiments in which the high-speed video (see Fig. 25) is used to image track the motion of ESM have demonstrated the efficacy of the technique, and the work is continuing to instrument the ESM with a dedicated IMU.

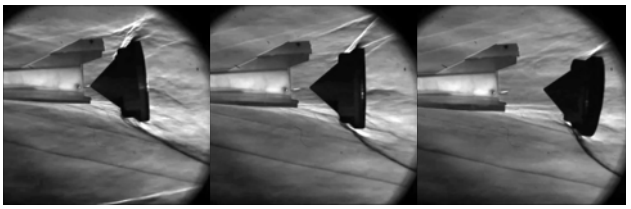

Fig. 25. Free flight separation of ESM from EFTV.

4 The Scramjet Vehicle Aerodynamics

4.1 CFD Activities and Results

TsAGI is performing CFD studies of the EFTV scramjet propelled configuration by using ANSYS-FLUENT and NUMECA CFD packages to raise the reliability of results. Both codes simulate the flow in the frame of RANS equations, with Spalart-Allmaras turbulence model when boundary layer (BL) is assumed turbulent (also laminar simulations are performed). Numerical simulations have been conducted in the range of $M_\infty = 5 \div 8$ and AoA = -2°÷8°. The Reynolds number is calculated on the airframe body length and corresponds to the values: $Re_L=6.88\cdot10^6$ ($M_\infty=5$), $Re_L=5.38\cdot10^6$ ($M_\infty=6$), $Re_L=7.66\cdot10^6$, $Re_L=7.33\cdot10^6$ ($M_\infty=7$) and $Re_L=5.92\cdot10^6$ ($M_\infty=8$). The computational grids of approximately 15-million elements are shown on Fig. 26, where the intake area and the beginning of the internal propulsive path are also detailed. Flow field analyses show a peculiarity of a significant subsonic zone (blue zones on pictures in Fig. 27), which occurs in the air intake central part. The turbulent simulations have shown generally stable and regular flow in the air intake area.

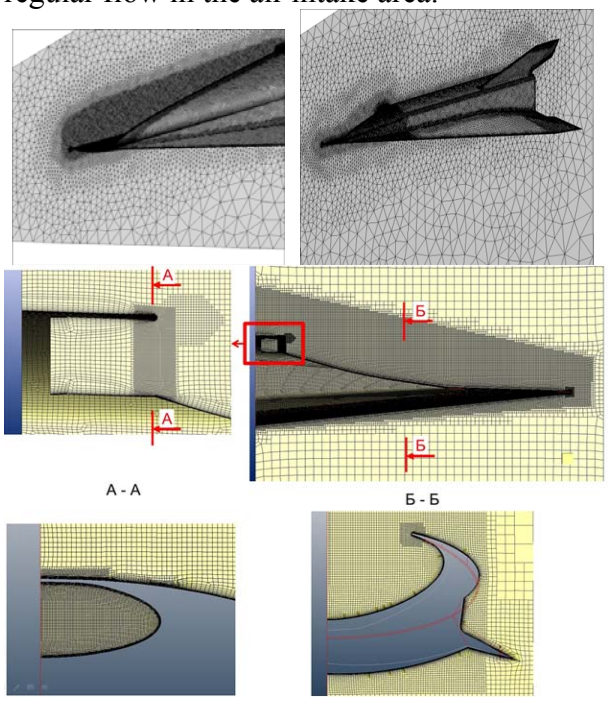

Fig. 26. Numerical grids for FLUENT (top) and NUMECA (down).

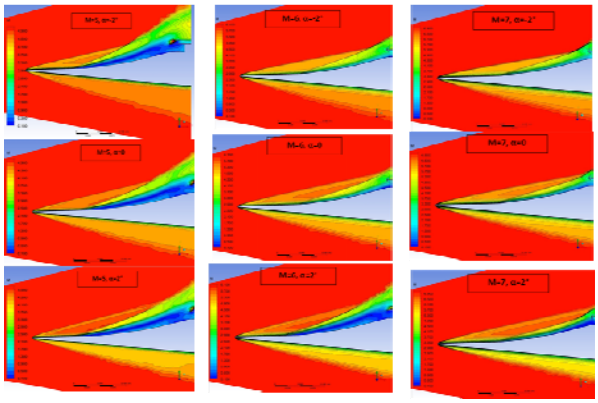

Fig. 27. FLUENT results: Mach number fields in the intake symmetry plane, M_∞=5, 6, 7, α=-2°, 0°, 2°.

In addition, high flow rate coefficients (f) throughout the considered range of Mach

numbers and AoA have been predicted.

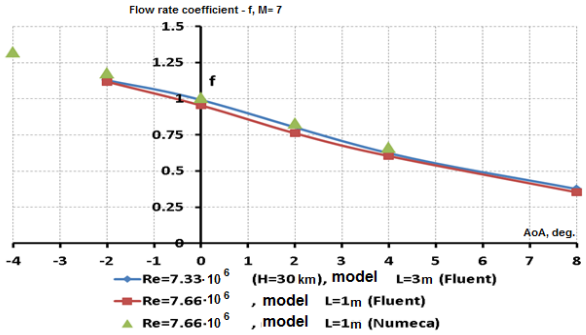

Fig. 28. Comparison of FLUENT and NUMECA results: the intake flow coefficient - f, M_∞=7.

For Mach numbers M_∞= 5, 7, 8 the flow coefficient decreases monotonically with increasing AoA (Fig. 28). It is important to note that when AoA=0° and Mach numbers are M_∞= 7, 8, the flow coefficient takes values close to 1, according to the results of both software packages ANSYS-FLUENT and NUMECA. At Mach M_∞= 6, a sharp decrease in the flow rate in the range of AoA= 0°÷2° was predicted resulting into an intake unstart.

A comparison of the Mach number contours at the inlet section, achieved by the two different codes, is shown in Fig. 29. The results indicate a good agreement for basic parameters: intake mass flow rate coefficient (f), density, pressure and Mach number.

Numerical simulation with the hypothesis of laminar boundary layer shows instability and, therefore, rising of the separation zone, which comes to the intake entrance and destroys its performance.

Fig. 30 shows the Mach number contours in the symmetry plane, obtained by ANSYS-FLUENT with turbulent and laminar boundary layer at M_∞=7 and AoA=0°. In the case of turbulent boundary layer, only a small local subsonic separation zone occurs on the intake surface. In case of laminar flow, a large separated subsonic region is visible, which extends downstream and blocks almost the whole intake entrance section.

Comparisons of data on the intake mass flow rate coefficient extracted from numerical simulations (with preset turbulent and laminar boundary layers) and the experimental data in the T-116 are shown in Fig. 31.

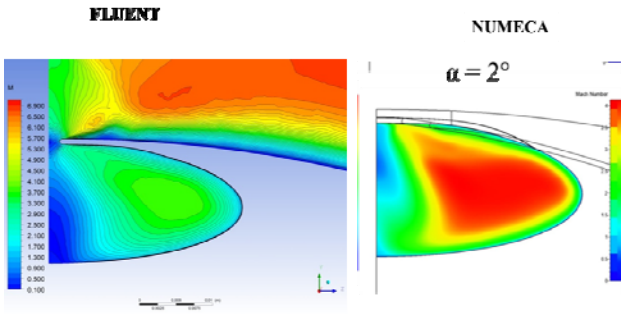

Fig. 29. Comparison of FLUENT and NUMECA results: Mach number contours at the intake entrance plane, M_∞=7, α=2°.

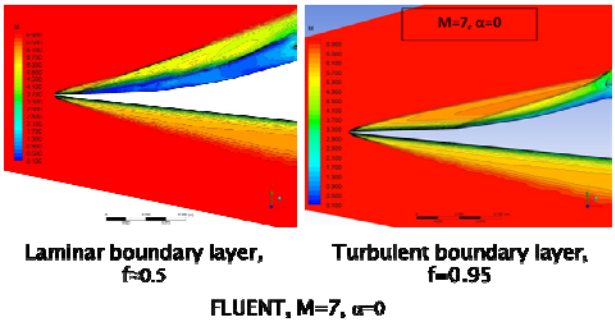

Fig. 30. Mach number contours: FLUENT results with laminar (left) and turbulent (right) boundary layer.

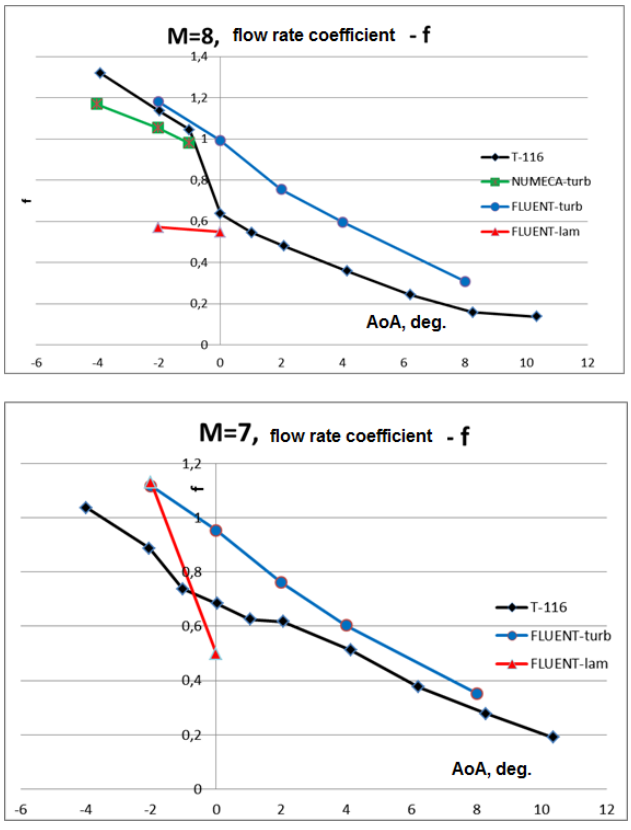

Fig. 31. The Intake Mass Flow Rate Coefficient: comparison of T-116 measurements with FLUENT results with turbulent and laminar boundary layers, M_∞= 7, 8.

The calculations with laminar boundary layer give significantly lower values of the flow coefficient ≈ 0.5 ÷ 0.6. These results are much closer to the experimental results without boundary layer tripping, which demonstrated low flow rate coefficient and intake unstart.

4.2 TsAGI Aerodynamic Tests on the EFTV Scramjet Propelled Option

TsAGI provides also experimental investigation on aerodynamics of the scramjet propelled option. Configuration of this option had been developed earlier in the HEXAFLY project [5][6], on the basis of the LAPCAT-MR2 hypersonic M_∞=8 hydrogen-fueled cruiser concept with dorsal inward-turning intake [3][4].

TsAGI produced an aerodynamic model of the EFTV propelled option at a 0.35 scale, i.e. approximately 1m long, which was tested in the TsAGI hypersonic wind tunnel T-116. The model was built with the internal duct to investigate the intake characteristics and to take into account the influence of the air passage through engine propulsive path on the external aerodynamics of the vehicle (see Fig. 32). The model was tested at Mach 6, 7 and 8.

Fig. 32. Aerodynamic model installed in the test section of TsAGI T-116 Wind Tunnel, EFTV scramjet propelled option.

The experimental results showed that the intake starting significantly depends on the boundary layer (BL) state, i.e. laminar, transitional or turbulent, over the intake compression surface. The first test series provided with 'clean' intake compression surface (without any BL transition grit) showed that starting of the intake appeared just in the very limited range of the test regimes, at Mach=8 and negative AoA ≤ – 1º. At Mach=7 and 6 the intake was not started.

The second test series was provided with different variants of transition grits, whose shapes are presented in Fig. 33. These included: 2 metallic strips with 3 rows of diamond-shaped roughness elements each; the heights of the roughness elements were 0.75 mm and 1 mm (var. 1), 10 screw heads of a 'dovetail' shape having the height k=1.4 mm and the top diameter D = 4 mm (var. 2), the same screw heads with wires of the diameter d = 0.5 mm attached to the model surface by the screws in 'cross' position (var. 3) and in 'lines' position, in parallel to the intake leading edge (var. 4).

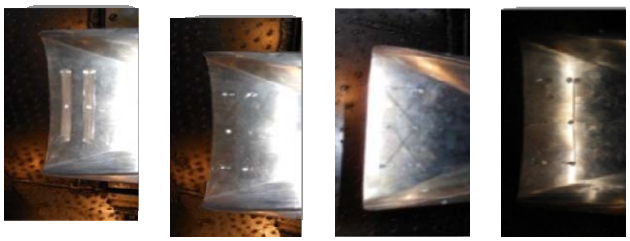

Var. 1 Var. 2 Var. 3 Var. 4

Fig. 33. Different variants of the BL transition grits used in the second test series.

The tests showed that transition grits' variants 2 to 4 led to significantly wider ranges of test conditions at which the intake was started.

The main test results obtained at Mach numbers 8 and 7 in terms of the intake mass flow rate coefficient f are shown in Fig. 34. Low values of f (less than approximately 0.6) indicate absence of the intake starting.

These results were obtained, however, with widened intake throat area corresponding to the intake contracting ratio CR = 7.8 which was lower than that of the original intake (CR = 8.6). Examining of the intake starting conditions for higher CR will be the main goal of further tests.

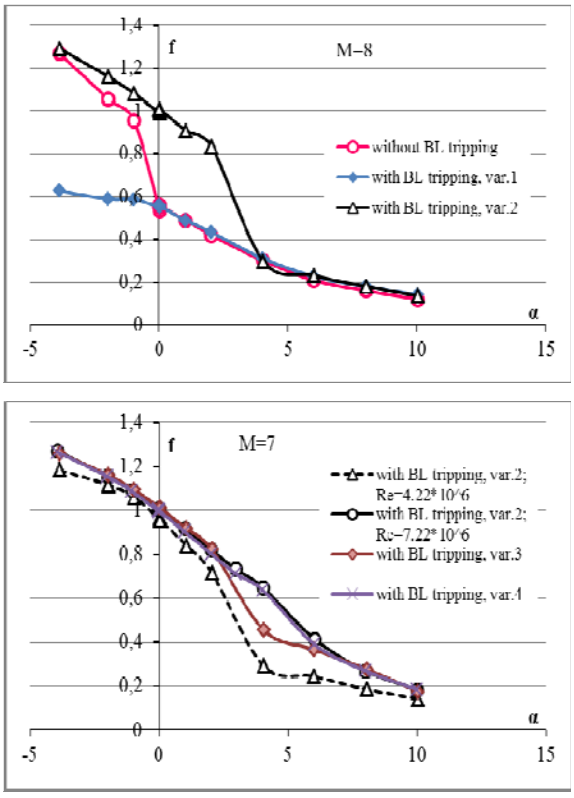

Fig. 34. Experimental data on the intake mass flow rate coefficient f at Mach Numbers 8 and 7.

4.3 Combustion Chamber Testing at the Connected-Pipe Facility T-131 TsAGI

TsAGI is also providing tests of the combustion chamber of the hydrogen-fuelled scramjet engine in the connected-pipe facility T-131. The model for these experimental tests was manufactured by CIAM, see Fig. 35.

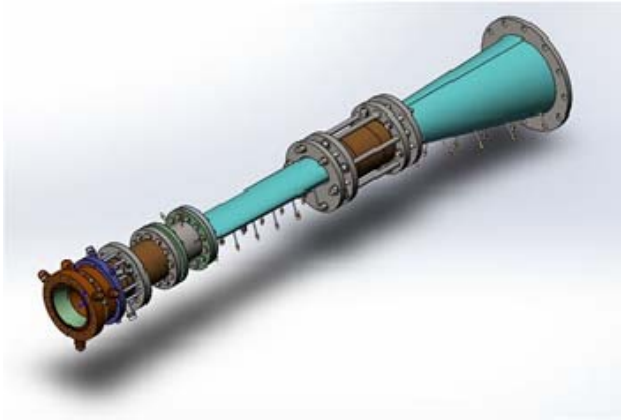

Fig. 35. Model of the hydrogen combustion chamber for testing at T-131 facility (TsAGI).

Main purpose of these experimental studies is to define the limits of stable operation of the combustion chamber. Beside this, it is also important to study the regimes at which self-ignition and flame stabilization are assured.

The model of the elliptical combustion chamber is a full-scale model fitting the actual size of the EFTV model. Such an approach makes it possible to conduct experimental investigations of the working principle without any adaptations. The combustion chamber to be tested when mounted on the connected-pipe facility is composed of the eight separate sections, interconnected through flanges (see Fig. 35): an intermediate part of the direct air heater, a part with critical section of the aerodynamic nozzle, supersonic part of the aerodynamic nozzle, a pre-injector section with two semi-struts, a section of combustion chamber with full-strut, a section of the 2D-nozzle and a section of the 3D-nozzle. The sealing of section is provided by the mark heat-resistant sealant. Full length of the model is L=2300 mm and weight of the model is approximately 300 kg.

In the course of fire tests, the static pressures are measured along the installation duct in 44 points (3 rows of measurements). The expected pressure values are in range of 0.1 to 1.5 bar, and the sensors rates are selected accordingly.

The T-131 facility (Fig. 36) is used mainly to study experimentally the operational process and the gas dynamics in ramjets and scramjets combustion chambers on the connected-pipe facility. The gas parameters in the air preheater of the test-bench allow simulating at the inlet of scramjet combustion chamber the total flow enthalpy, the M number and the pressure of flights in Mach number range 3 ÷ 10.

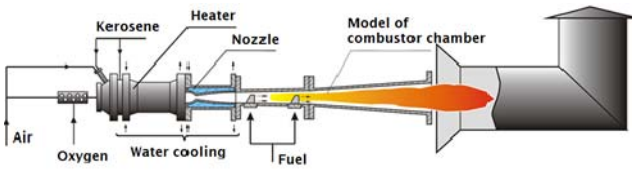

Fig. 36. Scheme of the T-131 facility.

The key component of the facility is a kerosene air heater of the gas-flame type. The air, the oxygen and the kerosene are supplied into the air heater combustion chamber in amount that is needed to create a flow with the

T_0 and p_0 predetermined stagnation parameters. It is to be noted that the oxygen is supplied into the air heater combustion chamber to replenish the burnt oxygen from air, in such a way that the oxygen portion in products of combustion be g_{ox}=0.232. The last requirement is of importance for simulating the atmospheric air when testing the processes of burning. Such a manner of compensation provides also the high completeness of kerosene burning.

Fig. 37 presents typical distribution of the static pressure along centreline of the model duct for Mach number M_∞=7, a simulated altitude of H=27÷28 km, with T_0=2100÷2150 K and equivalence ratio ER≈0.67. Pressure distribution is plotted before fuel supply (fuel-off, green squares) and during fuel supply (fuel-on, red triangles). On the X-axis is represented the distance from semi-struts in millimeters, and the Y-axis represents static pressure in bars.

One could see that when hydrogen is being supplied, the static pressure raises 4÷4.5 times in comparison with regime without hydrogen. This clearly proves that the fuel is burning inside model of the combustion chamber.

Besides this, it could be observed that main heat release takes place in section with full-strut and 2D nozzle section, but practically does not influence the 3D nozzle section.

However, it is worth noting that maximum of the static pressure inside the model is located in the section of the combustion chamber near full-strut or after it. Thus, it is indirectly proved that burning of hydrogen injected from semi-struts could start in the area nearby full-strut.

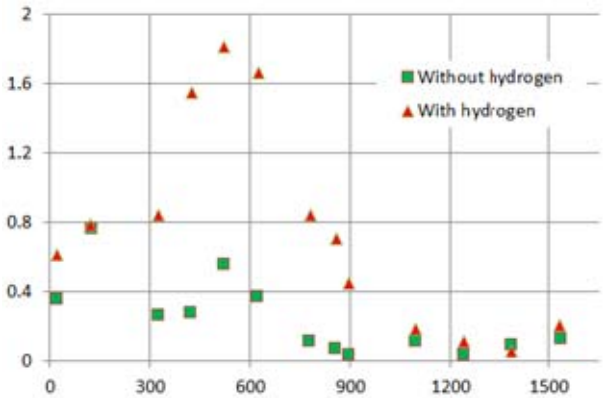

Fig. 37. Distribution of the static pressure at the centerline of the model.

4.4 CIAM Tests of the EFTV Full-Scale Scramjet Module in the C-16VK Facility

The full-scale EFTV scramjet module (Fig. 38) was designed and produced by CIAM. The scramjet module was designed for high-enthalpy testing and it consists of five main different parts: 1) air-intake with fuel pylon-injector; 2) combustion chamber; 3) nozzle; 4) frame; 5) power pylon.

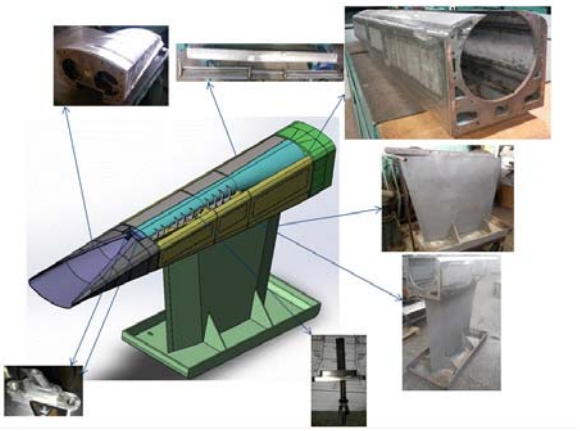

Fig. 38. The full-scale EFTV scramjet module.

Experimental research of the full-scale 3m long EFTV scramjet module was carried out in the CIAM ground test facility C-16VK, whose scramjet module installation in the facility is shown in Fig. 39. The purpose of these tests was the study of the operating conditions in the combustion chamber and EFTV scramjet propelled option aero-propulsive balance demonstration.

Fig. 39. Scramjet module installation in the facility.

Prior the execution of the experimental campaign, a computational analysis was carried out to obtain the operating conditions for air-intake starting. The mesh was generated for 3D model of scramjet module mounted to the test bench. A one-equation Spalart-Allmaras eddy viscosity model was used for turbulence modelling. The thermo-physical properties of gas used in numerical analysis are equal to fired heater combustion products properties.

A sequence of numerical computations of EFTV scramjet module in the test bench with contoured and conical nozzles were made. The contoured nozzle accelerates the flow up to M=7, the conical nozzle up to M=7.5.

As a result, the air-intake was started during all investigated regimes.

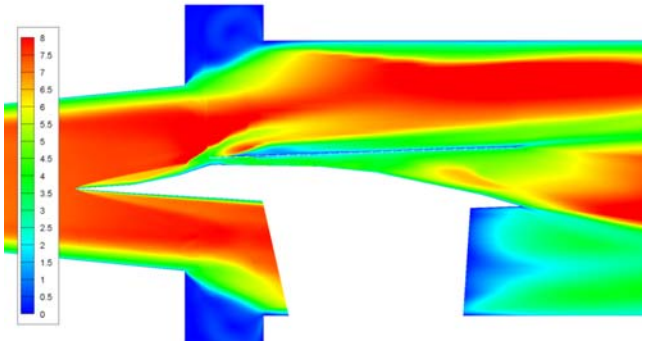

Fig. 40. Mach number contours in the symmetry plane for EFTV module flow in C-16VK facility conditions.

The numerical simulation results of EFTV module flow in the test bench with the conical nozzle at p*=64 bar and T*=2310 K is presented in Fig. 40. The intake is started, and no detached shock wave ahead of combustion chamber inlet is detected. Pressure and drag forces along the inner duct, the model outbound and power pylon are presented in Tab. 2.

	Inner duct	Outbound	Outbound with pylon	Module
Pressure drag force, N	242,0	-287,6	-348,4	-106,4
Viscous drag force, N	-142,0	-101,5	-146,0	-288,0
Total force, N	100,0	-389,1	-494,4	-394,4

Tab. 2. Pressure and drag forces effecting the object.

The total force obtained in numerical simulation was compared with the experimental one, whose value with no fuel injection is -370 N. This 6% difference demonstrates an adequate accuracy of the calculation method.

The experiments were conducted by applying a contoured nozzle for Mach number M_∞=7 in the outlet cross-section, and a conical nozzle for Mach number M_∞=7.4. The module was mounted on the thrust-measuring platform to determine the aero-propulsive balance. The main series of experiments was carried out with flow parameters corresponding to a flight altitude of the vehicle of H_∞=33 km. Particular attention was paid to dependencies of scramjet thrust from the equivalence ratio (ER) and mass flow rate schedule among the struts.

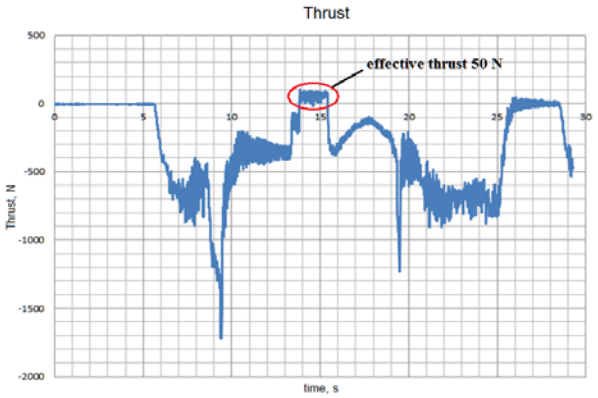

Fig. 41. Effective thrust to time dependence.

Positive aero-propulsive balance was demonstrated when the equivalence ratio ER was higher than 1.4. Effective thrust time history for ER=1.58 regime is shown in Fig. 41.

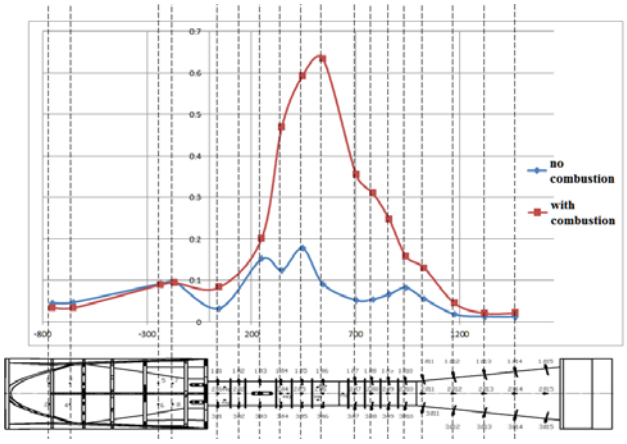

Fig. 42. Pressure distribution along the duct.

For combustion analysis, measured pressure distributions along the duct were obtained. In Fig. 42, pressure distributions for combustion and no combustion cases are shown. High pressures in the duct in fuel supply case indicate clearly presence of combustion, while average flow is supersonic along the whole duct.

5 Conclusions

The development status of both a high-speed glider and a propelled concept were described.

The feasibility of a flight experiment for a glider concept in all its phases was discussed on the basis of numerical results and windtunnel campaigns. The use of a sounding rocket, a release at an apogee of 90km followed by a pull-out manoeuvre allows flight testing the glider at Mach 7-8 at a flight altitude of about 30km.

The aero-propulsive performance of the propelled concept was also investigated numerically and experimentally. The outcome of the study indicated a positive thrust generation at these high speeds. The intake was shown to be sensitive to the transition location and needed to be triggered on the small scale to assure a representative flow field as for the envisaged passengers' vehicle.

The next steps are now directed towards the detailed design of the glider concept for the planned flight experiment. Based on the availability of the booster, the flight is planned for 2019.

Acknowledgements

This work was performed within the 'High Speed Experimental Fly Vehicles - International' (HEXAFLY-INT) project fostering International Cooperation on Civil High-Speed Air Transport Research. HEXAFLY-INT, coordinated by ESA-ESTEC, is supported by the EU within the 7th Framework Program Theme 7 Transport, Contract no.: ACP3-GA-2014-620327. The project is also supported by the Ministry of Industry and Trade, Russian Federation. Further information on HEXAFLY-INT can be found on http://www.esa.int/techresources/hexafly_int.

References

[1] Steelant J., "ATLLAS: Aero-Thermal Loaded Material Investigations for High-Speed Vehicles", *15th AIAA International Space Planes and Hypersonic Systems and Technologies Conference*, 28 April-1 May, 2008, Dayton, Ohio, USA, AIAA-2008-2582.

[2] Bouchez M., Dufour E., Le Naour B., Wilhelmi C., Bubenheim K., Kuhn M., Mainzer B., Riccius J., Davoine C. Justin J.-F., von Wolfersdorf J. Axtmann M., Villace F. and Steelant J., "Combustor Materials Research Studies for High Speed Aircraft in the European Program ATLLAS2", *20th International Space Planes and Hypersonic Systems and Technology Conference*, 5-8 July 2015, Glasgow, Scotland, UK, AIAA-2015-3639.

[3] Steelant, J., Varvill, R., Defoort, S., Hannemann, K., and Marini, M., "Achievements Obtained for Sustained Hypersonic Flight within the LAPCAT-II project", *20th AIAA International Space Planes and Hypersonic Systems and Technologies Conference*, Glasgow, Scotland, July 6-9, 2015, AIAA-2015-3677.

[4] Meerts, C., Steelant, J., "Air Intake Design for the Acceleration Propulsion Unit of the LAPCAT-MR2 Hypersonic Aircraft", in *5th European Conference for Aeronautics and Space Sciences (EUCASS)*, Munich, July 1-5, 2013.

[5] Pezzella, G., Marini, M., Cicala, M., Vitale, A., Langener, T., Steelant, J., "Aerodynamic Characterization of HEXAFLY Scramjet Propelled Hypersonic Vehicle", *32nd AIAA Aviation (Applied Aerodynamics Conference)*, 16-20 June 2014, Atlanta, GA, USA, AIAA 2014-2844.

[6] Steelant, J., Langener, T., Di Matteo, F., Hannemann, K., Riehmer, J., Kuhn, M., Dittert, C., Scheuerpflug, F., Jung, W., Marini, M., Pezzella, G., Cicala, M., Serre, L., "Conceptual Design of the High-Speed Propelled Experimental Flight Test Vehicle HEXAFLY", *20th AIAA International Space Planes and Hypersonic Systems and Technologies Conference*, Glasgow, Scotland, UK, 6-9 July 2015, AIAA-2015-3539.

[7] Favaloro, N., Rispoli, A., Vecchione, L., Pezzella, G., Carandente, V., Scigliano, R., Cicala, M., Morani, M., Steelant, J., "Design Analysis of the High-Speed Experimental Flight Test Vehicle HEXAFLY-International", *20th AIAA International Space Planes and Hypersonic Systems and Technologies Conference*, Glasgow, Scotland, UK, 6-9 July 2015, AIAA-2015-3607.

[8] Pezzella, G., Marini, M., Reimann, B., Steelant, J., "Aerodynamic Design Analysis of the Hexafly-INT Hypersonic Glider", *20th AIAA International Space Planes and Hypersonic Systems and Technologies Conference*, Glasgow, Scotland, UK, 6-9 July 2015, AIAA-2015-3644.

[9] Pezzella, G., Carandente, V., Scigliano, R., Marini, M., Steelant, J., "Aerothermal Environment Methodology of the Hexafly-Int Experimental Flight Test Vehicle (EFTV)", *8th European Symposium on Aerothermodynamics for Space Vehicles*, ESA, 2-6 March 2015, Lisbon, Portugal.

[10] Carandente, V., Scigliano, R., Pezzella, G., Marini, M., and Steelant, J., "Finite Element Thermal Design of the Hexafly-INT Experimental Flight Test Vehicle", *6th European Conference for Aeronautics and Space Sciences (Eucass)*, 29 June-3 July, 2015, Krakow, Poland.

[11] Riemann B., "Numerical Simulation of the Free Pitch Oscillation for a Re-entry Vehicle in Transonic Wind Tunnel Flow", *8th European Symposium on Aerothermodynamics for Space Vehicles*, ESA, 2-6 March 2015, Lisbon, Portugal.

[12] Pezzella G., van Brummen S., Steelant, J., "Assessment of Hypersonic Aerodynamic Performance of the EFTV-ESM Configuration in the Framework of the Hexafly-Int Research Project", *8th European Symposium on Aerothermodynamics for Space Vehicles*, ESA, 2-6 March 2015, Lisbon, Portugal.

[13] Steelant J. and Langener T., "The LAPCAT-MR2 Hypersonic Cruiser Concept", ICAS-2014-0428, *29th Congress of the International Council of the Aeronautical Sciences*, St. Petersburg, Russia, September 7-12, 2014.

[14] Kennell C., Neely A., O'Byrne S, Buttsworth D., "Measurement of Vehicle Stability Coefficients in Hypersonic Wind Tunnels", *20th AIAA International Space Planes and Hypersonic Systems and Technologies Conference*, Glasgow, Scotland, UK, 6-9 July 2015, AIAA-2015-3690.

[15] Kennell C., Neely A., Tahtali M., Buttsworth D.R., Choudhury R., "Free Flight Testing in Hypersonic Flows: HEXAFLY-INT EFTV", *AIAA SciTech*, AIAA 2016-1088.

[16] Buttsworth D.R., "Ludwieg Tunnel Facility with Free Piston Compression Heating for Supersonic and Hypersonic Testing", *9th Australian Space Science Conference 2009*, Published 2010.

Contact Author Email Address

The contact author is Marco Marini, CIRA, whose e-mail is m.marini@cira.it.

Copyright Statement